NOTICE: This is the author's version of a work that was accepted for publication in Soil Dynamics and Earthquake Engineering. Changes resulting from the publishing process, such as peer review, editing, corrections, structural formatting, and other quality control mechanisms may not be reflected in this document. Changes may have been made to this work since it was submitted for publication. A definitive version was subsequently published in Soil Dynamics and Earthquake Engineering, Vol. 75, pp. 199-210, 2015, DOI: 10.1016/j.soildyn.2015.04.008

Inspection of a high-cycle accumulation model for large numbers of cycles (N = 2 million)

T. Wichtmann[i)], Th. Triantafyllidis[ii)]

Abstract: The high-cycle accumulation (HCA) model for sand proposed by Niemunis et al. [16] has been developed based on numerous drained cyclic triaxial tests with 100,000 cycles. In the present paper the validity of the HCA model, in particular its function f_N and flow rule $\mathbf{m}$, for larger numbers of cycles is inspected. For that purpose, drained long-term cyclic triaxial tests with 2 million cycles have been performed on 13 clean quartz sands with different grain size distribution curves. For all tested sands, the function f_N, describing the shape of the strain accumulation curves $\varepsilon^{\mathrm{acc}}(N)$, has been found suitable up to 2 million cycles. The same applies to the cyclic flow rule $\mathbf{m}$, determining the ratio of the volumetric and deviatoric strain accumulation rates. Based on the data from the long-term tests, correlations between the HCA material parameters entering f_N and characteristics of the grain size distribution curve (d_{50}, C_u) have been improved for the application to 2 million cycles. These correlations are suitable for a simplified calibration of the HCA model and were validated up to 100,000 cycles only so far.

CE Database subject headings: long-term cyclic triaxial tests, 2 million cycles, high-cycle accumulation (HCA) model, quartz sand

1 Introduction

The residual deformations of foundations under high-cyclic loading, involving many cycles ($N \geq 10^3$) with relatively small strain amplitudes ($\varepsilon^{\mathrm{ampl}} \leq 10^{-3}$), can be predicted using empirical settlement formulas [8, 9, 12, 19], engineer-oriented models [2, 13, 24] or high-cycle accumulation (HCA) models [1,3,6,11,15–17,20–22]. Furthermore, several empirical formulas have been also developed in the field of pavement engineering, dedicated to the prediction of permanent deformations in pavements caused by traffic loading (e.g. [5, 10, 14, 18, 25, 26]). Owing to the long duration, most laboratory experiments or model tests utilized for a development or calibration of these mathematical models have been performed with numbers of cycles lying in the range $1,000 \leq N \leq 100,000$. However, many practical problems with high-cyclic loading involve a much larger number of load cycles ($N > 10^6$). For example, the foundations of offshore wind power plants are subjected to a very huge number of load cycles due to wind and wave action. Applications in pavement engineering also usually involve a number of load repetitions exceeding $N = 10^5$ by far. Unfortunately, only a very limited number of experimental studies has been performed with one million load cycles or more (e.g. [1,4,6,7,23]). Consequently, it is unclear so far if the various models proposed in the literature are suitable for such large numbers of cycles.

Different functions are used within the models in order to describe the increase of settlement s, pile head deflection y or residual strain $\varepsilon^{\mathrm{acc}}$ with increasing number of cycles N. A logarithmic relationship

$$\varepsilon^{\mathrm{acc}} \sim \ln(1 + a\ N) \tag{1}$$

and a power law

$$\varepsilon^{\mathrm{acc}} \sim N^b \tag{2}$$

with parameters a and b are the two most wide-spread approaches. The HCA model proposed by Niemunis et al. [16] uses a combination of a logarithmic and a linear function:

$$\varepsilon^{\mathrm{acc}} \sim f_N = C_{N1}\,[\ln(1 + C_{N2}N) + C_{N3}N] \tag{3}$$

with parameters C_{N1}, C_{N2} and C_{N3}.

Based on drained cyclic triaxial tests with 10^5 cycles it has been demonstrated in [28,31] that Eq. (3) - in contrast to Eqs. (1) and (2) - is able to fit the experimentally observed accumulation curves $\varepsilon^{\mathrm{acc}}(N)$ for clean quartz sand or gravel with various grain grain size distribution curves. As an example, Figure 1 presents $\varepsilon^{\mathrm{acc}}(N)$ data measured for a poorly graded medium coarse sand (Figure 1a), a poorly graded fine gravel (Figure 1b) and a well-graded sand (Figure 1c). The logarithmic function (1), given as dashed curves in Figure 1, can be fitted well to the experimental data of the poorly graded fine gravel (Figure 1b). In the range $N \leq 10^4$ it is also suitable for the poorly graded medium coarse sand (Figure 1a). However, Eq. (1) is inappropriate for the well-graded sand since the experimental curve $\varepsilon^{\mathrm{acc}}(N)$ shows a pronounced bending if plotted in a diagram with semi-logarithmic scale (Figure 1c). Furthermore, Eq. (1) is also unable to reproduce the $\varepsilon^{\mathrm{acc}}(N)$ data for the uniform medium coarse sand at higher numbers of cycles $N > 10^4$ (Figure 1a). The power-law function (2) approximates well the data for the well-graded material (see the dot-dashed curve in Figure 1c), but its fitting to

[i)] Research Assistant, Institute of Soil Mechanics and Rock Mechanics (IBF), Karlsruhe Institute of Technology (KIT), Germany (corresponding author). Email: torsten.wichtmann@kit.edu

[ii)] Professor and Director of the IBF, KIT, Germany

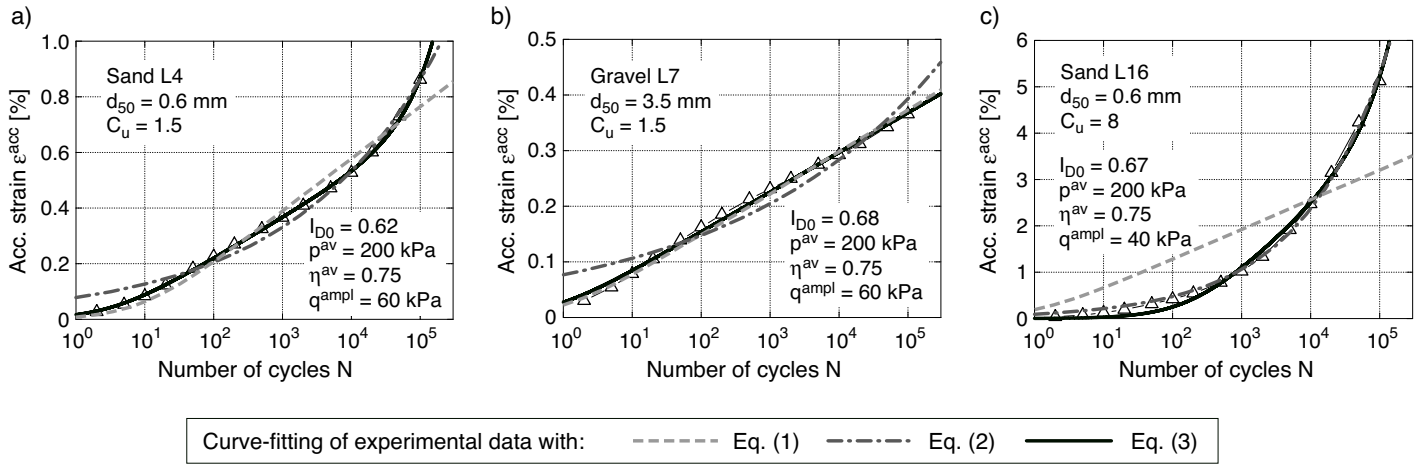

Fig. 1: *Accumulation curves $\varepsilon^{acc}(N)$ measured for granular materials with different grain size distribution curves in drained cyclic triaxial tests with 10^5 cycles of constant stress amplitude. Eqs. (1), (2) and (3) were fitted to the experimental data.*

the data of the poorly graded materials (Figure 1a,b) is non-satisfying. In contrast, Eq. (3) shown as solid curves in Figure 1, is flexible enough to describe sufficiently well the measured $\varepsilon^{acc}(N)$ curves for the various grain size distribution curves. Therefore, using Eq. (3) in a HCA model enables an application to a wide range of granular materials.

However, nearly all drained cyclic triaxial tests performed in the context of the HCA model of Niemunis et al. [16] so far [28,30,31] were restricted to 10^5 cycles. Therefore, the function f_N according to Eq. (3) is confirmed up to $N = 10^5$ only. The same applies to the cyclic flow rule $\mathbf{m}$, which determines the partition of the rate of strain accumulation $\dot{\varepsilon}^{acc}$ into a volumetric ($\dot{\varepsilon}_v^{acc}$) and a deviatoric ($\dot{\varepsilon}_q^{acc}$) portion.

The present paper examines whether the present formulations for f_N and $\mathbf{m}$ are appropriate also for larger numbers of cycles. The data from drained long-term cyclic triaxial tests with 2 million cycles performed on 13 clean quartz sands with different grain size distribution curves are analyzed for that purpose.

2 Tested materials and testing procedure

A single cyclic triaxial test has been performed on each of the 13 specially mixed grain size distribution curves shown in Figure 2. These mixtures were already used for the experimental work documented in [30, 31]. The raw material is a fluvially deposited natural quartz sand obtained from a sand pit near Dorsten, Germany. It has a grain density of $\varrho_s = 2.65$ g/cm^3. The sands L2 to L7 (Figure 2a) have the same uniformity coefficient $C_u = 1.5$ but different mean grain sizes in the range 0.2 mm $\leq d_{50} \leq$ 3.5 mm. The materials L4 and L10 to L16 (Figure 2b) have the same mean grain size $d_{50} = 0.6$ mm but different uniformity coefficients $1.5 \leq C_u \leq 8$. The index properties of the 13 sands are summarized in Table 1.

The raw material used for the mixtures has a subangular grain shape. For five different grain sizes, photos of the grains taken with an optical microscope are provided in Figure 3. The grain shape has been further analyzed on the basis of images of the grains taken with a flat bed scanner (resolution 9600 dpi). These images were converted to a black-and-white format before being analyzed using the

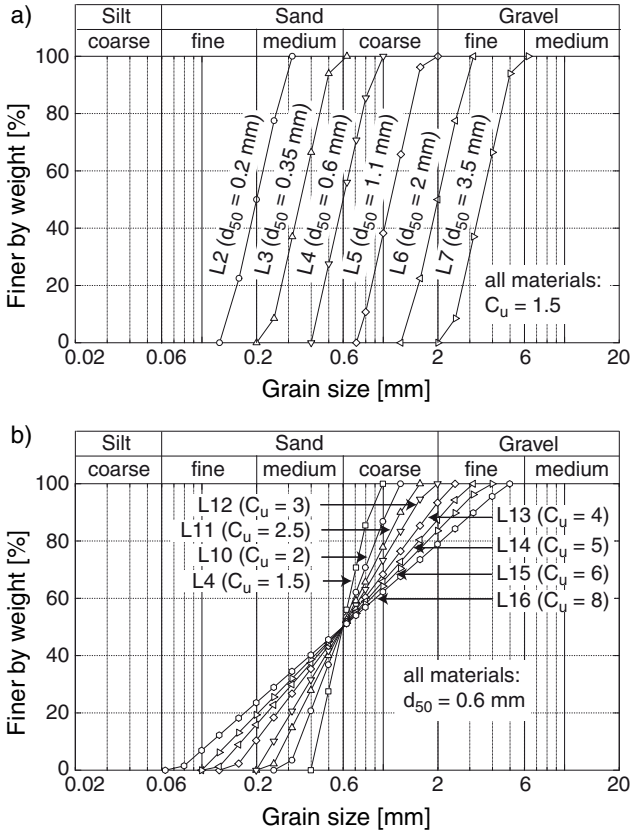

Fig. 2: *Tested grain size distribution curves*

software ImageJ with the Plugin Particles 8. All particles on the figure having a size in accordance with the grain fraction under consideration (no dust particles or similar should be analyzed) and lying separately (i.e. without any contact to neighboured grains, in order to prevent the analysis of conglomerates of several grains) were identified. The cross-sectional area, perimeter, geometric centre of gravity, etc. of the individual grains measured in pixels were determined. Based on this information, several geometric parameters describing the shape of the particles could be calculated. For example, Aspect Ratio is defined as the ra-

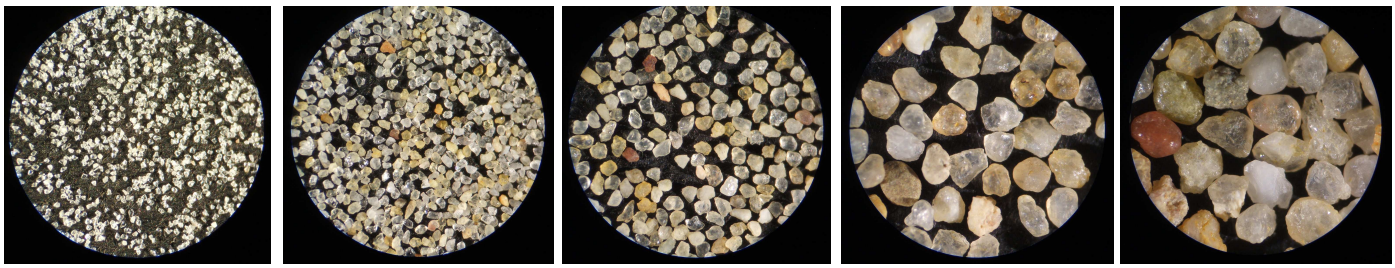

0.063 ÷ 0.08 mm | 0.125 ÷ 0.16 mm | 0.20 ÷ 0.25 mm | 0.50 ÷ 0.63 mm | 0.71 ÷ 0.80 mm

Fig. 3: Photos of the grains of different fractions of the raw material used for the mixtures taken by means of an optical microscope (circular opening corresponds to a length of 25 mm)

Sand	d_{50} [mm]	C_u [-]	C_c [-]	$e_{\min}$ [-]	$e_{\max}$ [-]	φ_c [°]
L2	0.2	1.5	0.9	0.596	0.994	32.9
L3	0.35	1.5	0.9	0.591	0.931	33.1
L4	0.6	1.5	0.9	0.571	0.891	32.8
L5	1.1	1.5	0.9	0.580	0.879	33.6
L6	2.0	1.5	0.9	0.591	0.877	35.0
L7	3.5	1.5	0.9	0.626	0.817	36.4
L10	0.6	2	0.9	0.541	0.864	33.1
L11	0.6	2.5	0.8	0.495	0.856	33.2
L12	0.6	3	0.8	0.474	0.829	33.6
L13	0.6	4	0.8	0.414	0.791	33.6
L14	0.6	5	0.7	0.394	0.749	33.1
L15	0.6	6	0.7	0.387	0.719	33.0
L16	0.6	8	0.7	0.356	0.673	33.2

Table 1: Index properties (mean grain size d_{50}, uniformity coefficient $C_u = d_{60}/d_{10}$, curvature index $C_c = d_{30}^2/(d_{10}d_{60})$, minimum and maximum void ratios $e_{\min}$, $e_{\max}$) for the 13 tested sands. φ_c is the critical friction angle determined as the angle of repose from a pluviated cone of sand.

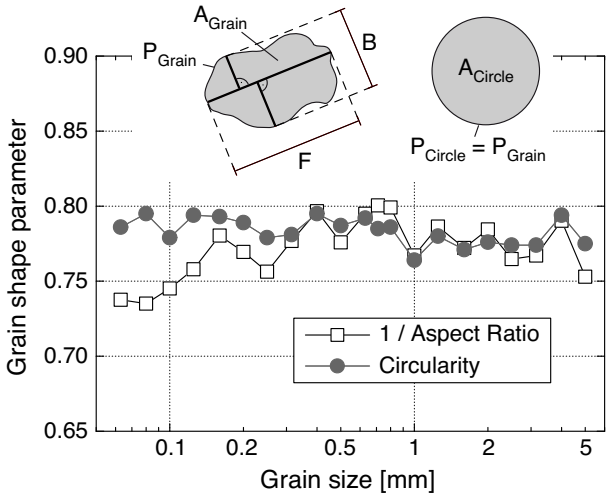

Fig. 4: *Grain shape parameters as a function of grain size: Aspect Ratio is defined as F/B and Circularity as A_{Grain}/A_{Circle}. A_{Grain} denotes the cross-sectional area of the grain, P_{Grain} its perimeter and A_{Circle} and P_{Circle} are the respective values of a circle having the same perimeter as the grain.*

tio of the length F of the longest axis divided by the length B of the largest dimension in the orthogonal direction (see schemes in Figure 4). Circularity is obtained as the ratio of the cross-sectional area of the grain A_{Grain} divided by the area A_{Circle} of a circle having the same perimeter as the original grain (Figure 4). Circularity is thus a measure of how much the shape of a grain resembles a circle. It should be kept in mind, however, that this analysis is restricted to two-dimensional images of the grains, not evaluating their third dimension.

For each fraction of the raw material, several hundreds of grains have been analyzed in this way. Mean values of the shape parameters of all grains within a fraction are considered further. In Figure 4 the reciprocal mean value of Aspect Ratio and the mean value of Circularity are plotted as a function of grain size. While Circularity is rather independent of grain size, a slight decrease of the Aspect Ratio in the range of grain sizes between 0.063 mm and about 0.3 mm can be concluded from Figure 4. At larger grain sizes, also Aspect Ratio is not significantly changing with increasing grain size. Therefore, the shape of the grains can be regarded as approximately similar for all granular mixtures tested in this study.

Owing to the long duration, the tests of the present study were run in four similar test devices simultaneously. The devices and their measurement technique are described e.g. in [31]. The cyclic axial loading was applied with a pneumatic loading device. The samples with a diameter of 10 cm and a height of 20 cm were prepared by air pluviation. All samples tested in the present study were medium dense ($0.59 \leq I_{D0} = (e_{\max} - e_0)/(e_{\max} - e_{\min}) \leq 0.73$). They were tested under water-saturated conditions using a back pressure of 200 kPa. The effective lateral stress $\sigma_3 = 150$ kPa was kept constant during all tests. The average effective axial stress was chosen as $\sigma_1^{\text{av}} = 300$ kPa for all samples, resulting in an average mean pressure of $p^{\text{av}} = 200$ kPa, an average deviatoric stress of $q^{\text{av}} = 150$ kPa and an average stress ratio of $\eta^{\text{av}} = q^{\text{av}}/p^{\text{av}} = 0.75$. The deviatoric stress amplitude was chosen as $q^{\text{ampl}} = 80$ kPa in the tests on materials L4 to L7, as $q^{\text{ampl}} = 60$ kPa for L2, L3, L10 and L11 and as $q^{\text{ampl}} = 40$ kPa for L12 to L16. The lower stress amplitudes for the finer and more well-graded sands accommodate the larger strain accumulation rates usually observed for those materials [28, 31]. Due to its larger deformation, the first *irregular* cycle was applied with a low frequency of 0.01 Hz in all tests. Afterwards, the samples were subjected to 2 million *regular* cycles with a frequency of 1 Hz.

Since the HCA model predicts the accumulation due to the regular cycles only, the first irregular cycle is not further

discussed in this paper. All data presented refers to the regular cycles, that means $N = 1$ refers to the end of the first regular cycle.

The long duration of the tests (approx. 23 days) implicated some technical problems. The diffusion of air into the pore water was prevented by using de-aired cell water and a layer of silicon oil on both the water in the cell and the water in the burette which was used for the volume change measurements [31]. Diffusion from cell water into the sample was delayed by applying a layer of silicon grease to the latex membrane (membrane thickness 0.4 mm, more impermeable butyl membranes were not available at the time of the testing). However, most of the tests showed some leakage of cell water into the sample after several days, which became visible as a more or less sharp bend in the $\varepsilon_v^{\mathrm{acc}}$-$\varepsilon_q^{\mathrm{acc}}$ strain paths (see the exemplary plot for sand L5 in Figure 5), where $\varepsilon_v^{\mathrm{acc}}$ and $\varepsilon_q^{\mathrm{acc}}$ are the accumulated volumetric and deviatoric strain. Only the tests on materials L2, L11 and L16 did not show any leakage during the 2 million cycles. While the residual volumetric strain data after leakage cannot be used for the analysis of the tests, the axial strain data is not affected by leakage. The degree of saturation of the samples is also not altered by leakage since both the pore and the cell water are de-aired.

3 Test results

3.1 Direction of accumulation - high-cyclic flow rule m

The $\varepsilon_v^{\mathrm{acc}}$-$\varepsilon_q^{\mathrm{acc}}$ strain paths measured in the long-term tests are presented in Figure 5. For a given test, the data markers shown in the diagrams of Figure 5 correspond to different numbers of cycles ($N = 1$, 2, 5, 10, 20, 50, ..., $2 \cdot 10^6$). The data after the start of leakage are not included in Figure 5. The only exception is the diagram for sand L5, where the strain path after the start of leakage is exemplarily shown.

For comparison, the strain paths measured in an earlier study [30] are included in Figure 5. In those tests with same average and cyclic stresses and similar initial densities, samples of the same sands had been subjected to 10^5 cycles only. Up to $N = 10^5$ the new and the old $\varepsilon_v^{\mathrm{acc}}$-$\varepsilon_q^{\mathrm{acc}}$ strain paths are in good accordance (Figure 5). The data from the new long-term tests in Figure 5, in particular those for sands L2, L11 and L16 where leakage did not occur during 2 million cycles, demonstrate that no significant change of the direction of the $\varepsilon_v^{\mathrm{acc}}$-$\varepsilon_q^{\mathrm{acc}}$ strain paths occurs after 100,000 cycles. This means that the direction of accumulation, i.e. the ratio $\dot{\varepsilon}_v^{\mathrm{acc}}/\dot{\varepsilon}_q^{\mathrm{acc}}$ of the volumetric and deviatoric strain accumulation rates, measured in the range $10^5 < N \leq 2 \cdot 10^6$ agrees well with that obtained for $N < 10^5$.

This is also evident in Figure 6 which compares the $\varepsilon_q^{\mathrm{acc}}(\varepsilon_v^{\mathrm{acc}})$ data at $N = 10^5$ (open symbols, obtained from both the old and new test series) with the data gathered at higher numbers of cycles $10^5 < N \leq 2 \cdot 10^6$ (filled symbols, corresponding to the last reliable data point in the long-term cyclic tests before leakage). In Figure 6 it is not distinguished between the various tested sands. Obviously, the open and the filled symbols in Figure 6 lie on a unique curve, confirming that the strain rate ratio $\dot{\varepsilon}_v^{\mathrm{acc}}/\dot{\varepsilon}_q^{\mathrm{acc}}$ is similar for $N \leq 10^5$ and $10^5 < N \leq 2 \cdot 10^6$. Furthermore, Figure 6 reveals that the direction of accumulation for the 13 tested granular materials is almost identical, at least at the tested stress ratio $\eta^{\mathrm{av}} = 0.75$.

Based on Figures 5 and 6 it can be concluded that the high-cyclic flow rule **m** of the HCA model is confirmed up to 2 million cycles. The equations for **m** found suitable for $N \leq 10^5$ (e.g. the flow rule of the Modified Cam-clay model or a more general flow rule proposed in [32], see a detailed discussion in [30]) are applicable also for larger numbers of cycles.

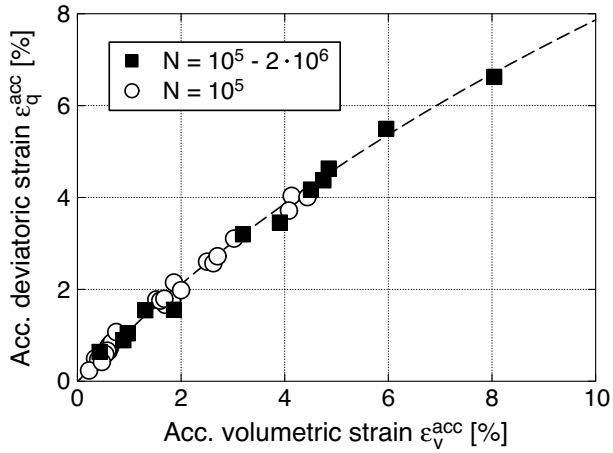

Fig. 6: *Accumulated deviatoric strain ε_q^{acc} versus accumulated volumetric strain ε_v^{acc}: Comparison of data at $N = 10^5$ (from old and new test series) and $10^5 < N \leq 2 \cdot 10^6$ (last reliable data point in the long-term tests before leakage). The diagram contains the data from all 13 tested granular materials.*

3.2 Intensity of accumulation - function f_N

The measured curves of permanent axial strain $\varepsilon_1^{\mathrm{acc}}$ versus the number of cycles are given in Figure 7. Up to $N = 10^5$, the new data agree well with those from the older test series [31] where only 10^5 cycles had been applied. For the poorly graded sands L2 to L5, the disproportional increase of $\varepsilon_1^{\mathrm{acc}}$ with $\ln(N)$ continues even up to $N = 2 \cdot 10^6$ cycles. Furthermore, also for the coarse sands and fine gravels L6 and L7, which obey $\varepsilon_1^{\mathrm{acc}} \sim \ln(N)$ in the range $N \leq 10^5$, a disproportional increase of $\varepsilon_1^{\mathrm{acc}}$ with $\ln(N)$ was observed at larger numbers of cycles $10^5 < N \leq 2 \cdot 10^6$. Therefore, while a logarithmic function $\varepsilon_1^{\mathrm{acc}} \sim \ln(N)$ may be suitable for coarse sand and fine gravel up to 10^5 cycles, it is inappropriate for larger numbers of cycles. For most of the more well-graded materials L10 to L16, the curves $\varepsilon_1^{\mathrm{acc}}(N)$ showed a pronounced bending in the semi-logarithmic diagrams up to 100,000 cycles, but were almost linear in the range $10^5 < N \leq 2 \cdot 10^6$. For some materials (e.g. L13, L14) a decrease of the rate of accumulation at $N > 10^6$ lead to S-shaped accumulation curves.

The new long-term cyclic triaxial tests have been recalculated using an element test program that simulates the development of permanent strain $\varepsilon_1^{\mathrm{acc}}$ with increasing number of cycles using the HCA model. The parameters C_{ampl}, C_e, C_p, C_Y, C_{N1}, C_{N2} and C_{N3} published in [31] have been applied in these simulations. These parameters are also provided in columns 2 to 8 of Table 2. They have been calibrated from several cyclic tests with 10^5 cycles performed with different stress amplitudes, initial soil densities and average stresses [31]. The average stress ($p^{\mathrm{av}} = 200$ kPa, $\eta^{\mathrm{av}} = 0.75$), the initial void ratio and the strain amplitudes $\varepsilon^{\mathrm{ampl}}(N)$ measured in the long-term tests were used as in-

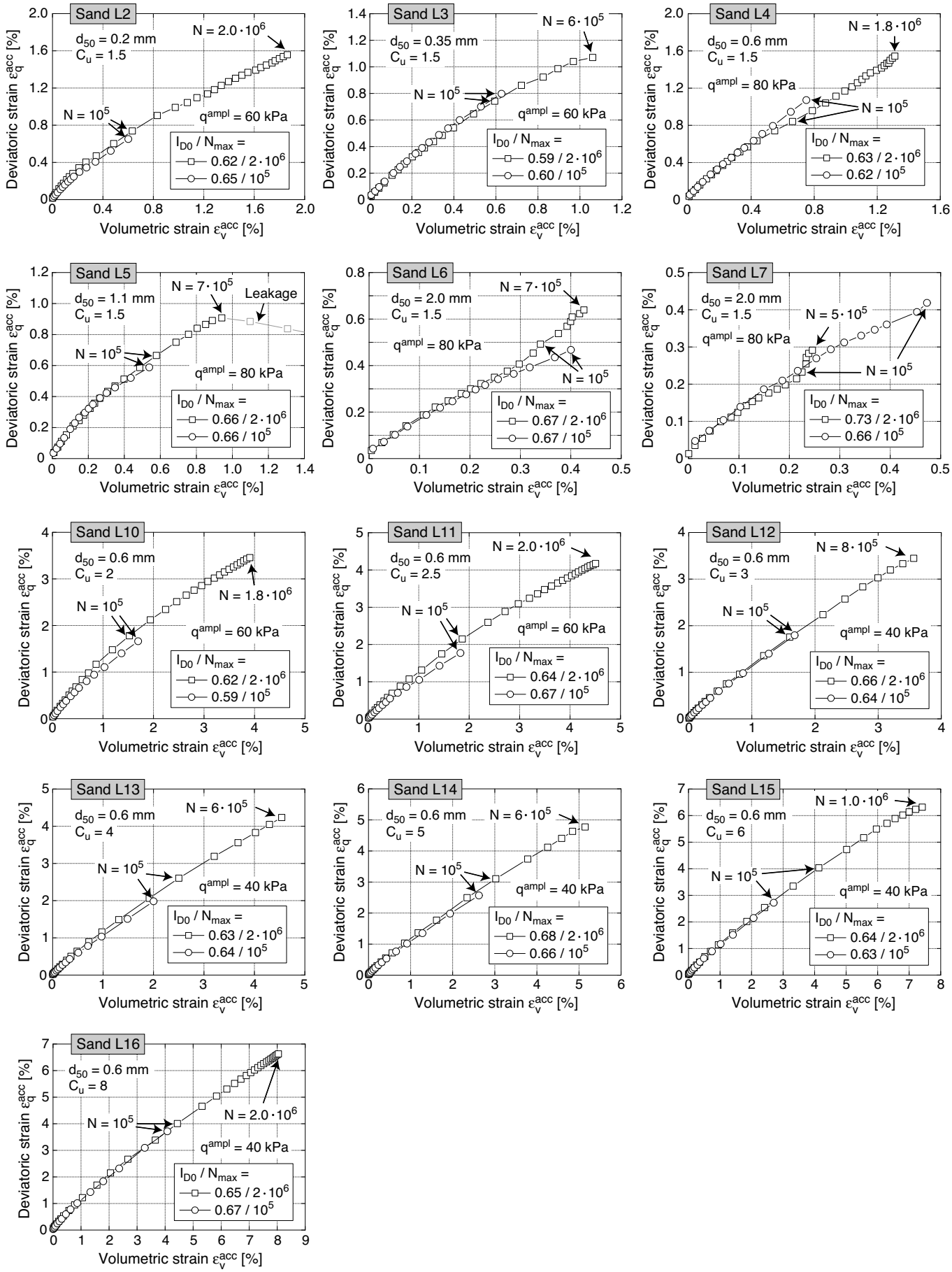

Fig. 5: ε_q^{acc}-ε_v^{acc} *strain paths measured in the tests with* $N = 2 \cdot 10^6$ *cycles. For comparison, data from an earlier test series [30] with* 10^5 *load cycles are also provided.*

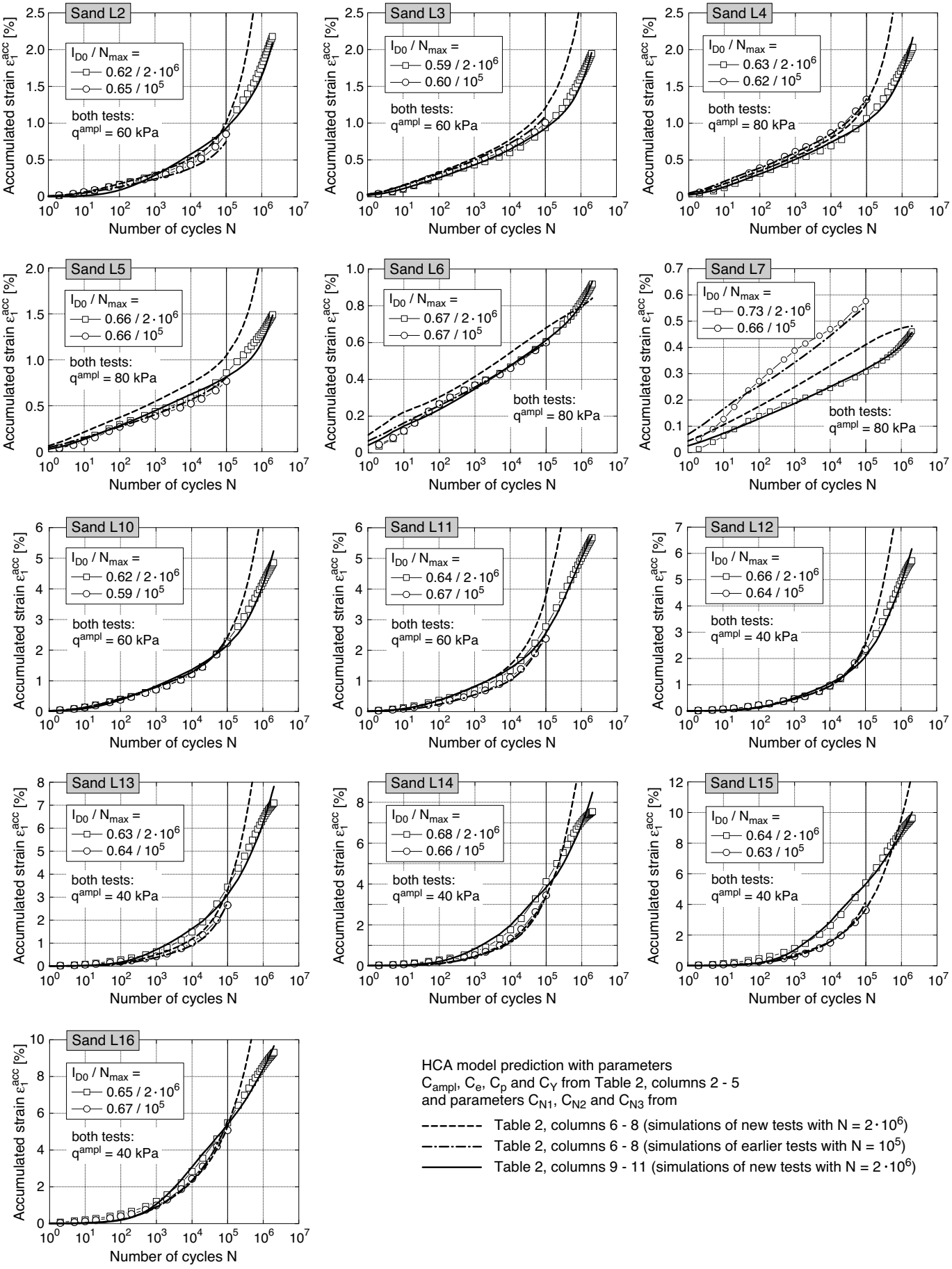

Fig. 7: *Accumulation curves $\varepsilon_1^{acc}(N)$ measured in the tests with $N = 2 \cdot 10^6$ cycles. For comparison, data from an earlier test series [31] with 10^5 load cycles are also provided.*

put for the recalculations (a detailed explanation on how $\varepsilon^{\mathrm{ampl}}$ and $\varepsilon^{\mathrm{acc}}$ are derived from the raw test data can be found in [29]). The predicted accumulation curves $\varepsilon_1^{\mathrm{acc}}(N)$ have been added as dashed curves in Figure 7. Curves obtained from a recalculation of the older tests with 10^5 cycles using the same sets of parameters are also provided in Figure 7 (dot-dashed curves). Obviously, for most tested materials the experimental data and the curves from the simulations agree sufficiently well up to $N = 10^5$ cycles. Somewhat larger differences were observed for materials L5, L7 and L15 which may be attributed to the usual scatter of data from cyclic tests. However, for most tested materials (L2 to L5 and L10 to L16), the permanent strains at larger numbers of cycles $N > 10^5$ are significantly overestimated by the parameters in columns 2 to 8 of Table 2 determined from the tests with $N \leq 10^5$. This can be primarily attributed to too large C_{N3}-values used in the function f_N according to Eq. (3). C_{N3} is of crucial importance for the accumulation rates at large number of cycles. Obviously, it can be inadequately determined from tests with 10^5 cycles.

Consequently, a new set of parameters C_{N1}, C_{N2} and C_{N3} for Eq. (3) has been calibrated based on the data from the tests with 2 million cycles. The parameters C_{ampl}, C_e, C_p, C_Y were adopted from the earlier test series (columns 2 to 5 of Table 2). The C_{Ni} parameters have been determined by means of an element test program described in detail in [31]. The program uses an automated optimization algorithm to find those parameters for which the sum of squared deviations between the measured and the predicted $\varepsilon_1^{\mathrm{acc}}(N)$ curves takes its minimum. The respective parameters are summarized in columns 9 to 11 of Table 2.

The HCA model prediction for the tests with 2 million cycles using these parameters has been added as solid curves in Figure 7. For most tested materials a relatively good agreement between the predicted and the experimental data is observed at $N > 10^5$. The only exception are the two materials L13 and L14, where the decrease of the accumulation rate at $N > 10^6$ is not reflected by the function f_N in combination with the functions f_e (decrease of $\dot{\varepsilon}^{\mathrm{acc}}$ due to compaction) and f_{ampl} (decrease of $\dot{\varepsilon}^{\mathrm{acc}}$ due to decreasing strain amplitude $\varepsilon^{\mathrm{ampl}}$, see Section 3.3) of the HCA model. In some cases the new set of parameters implies some loss of prediction accuracy in the range $N < 10^5$, becoming evident as a larger deviation of the predicted curve from the measured $\varepsilon^{\mathrm{acc}}$ data in certain ranges of N. For example, in case of L2, the predicted curve lies slightly below the measured data up to $N = 10^3$ and slightly above in the range $10^3 < N < 10^5$. In that case, a better approximation of the data for $N \leq 10^5$ could be achieved with a set of parameters fitted exclusively to the data in that range. Despite these somewhat larger deviations in the range of low N-values it can be concluded that the function f_N of the HCA model according to Eq. (3) is approximately adequate up to 2 million cycles, for all grain size distribution curves tested in the present study. The data for sands L13 and L14 at $N > 10^6$ give hints, however, that this conclusion may not be applicable to even larger numbers of cycles. Tests with $N \gg 2 \cdot 10^6$ would be necessary to clarify that issue.

The dependence of the intensity of strain accumulation on the grain size distribution curve is inspected based on the data from the new long-term cyclic tests. The diagram in Figure 8a collects the axial strain accumulation curves measured for all uniform materials (L2 - L7) with $C_u = 1.5$ and various d_{50} values between 0.2 and 3.5 mm, while the $\varepsilon_1^{\mathrm{acc}}(N)$ data for all sands with $d_{50} = 0.6$ mm and different uniformity coefficients in the range $1.5 \leq C_u \leq 8$ (L4, L10 - L16) are summarized in Figure 8b. The diagrams in Figure 8c,d present the residual strain $\varepsilon_1^{\mathrm{acc}}$ after 100,000 and 2 million cycles as a function of mean grain size d_{50} (Figure 8c, data of L2 - L7) or uniformity coefficient C_u (Figure 8d, data of L4, L10 - L16), respectively. The jumps in the data provided in Figure 8c,d are due to the different stress amplitudes chosen in the tests on the different materials. Although three different amplitudes $q^{\mathrm{ampl}} = 40$, 60 and 80 kPa have been applied for the 13 tested materials, a decrease of the intensity of strain accumulation with increasing mean grain size and an increase of $\dot{\varepsilon}^{\mathrm{acc}}$ with C_u is obvious in the various representations in Figure 8. These findings from the new long-term tests agree well with the results from the earlier study documented in [31]. For a discussion of possible reasons of the d_{50}- and C_u-influence it is referred to [31].

Figure 9 analyzes the development of relative density I_D during the tests. Initially, all samples were medium dense. Since the leakage addressed above affects the volumetric strain measurement, the void ratio and relative density values after the occurrence of leakage were evaluated under the assumption (justified by the analysis in Section 3.1) that the strain rate ratios $\dot{\varepsilon}_v^{\mathrm{acc}}/\dot{\varepsilon}_q^{\mathrm{acc}}$ before and after leakage are identical. In congruence with the $\varepsilon_1^{\mathrm{acc}}$ data presented in Figure 8, the diagrams in Figure 9b,d reveal that the reduction of relative density becomes more pronounced with increasing uniformity coefficient of the tested material. Relative densities slightly below or even above 1.0 have been reached in case of the well-graded materials L15 and L16 ($C_u = 6$ or 8, respectively) at $N = 2 \cdot 10^6$. According to the HCA model equations, reflecting the experience from tests with different initial relative densities [27, 28, 31], the strain accumulation vanishes ($\dot{\varepsilon}^{\mathrm{acc}} = 0$) when the void ratio reaches $e = C_e$, due to $f_e = 0$. Usually, C_e is slightly lower than the minimum void ratio e_{min} obtained from standard tests. Therefore, relative densities $I_D > 1$ can be reached under a drained high-cyclic loading. This is confirmed by the actual data for material L16. However, it can be expected that the strain accumulation rate strongly declines when e approaches C_e. The S-shaped accumulation curves observed during the final stage of the tests on L13 and L14 may already reflect such approximation of the densest possible state. Similar S-shaped curves would probably have been obtained for L15 and L16 if the cyclic loading would have been continued above $N = 2 \cdot 10^6$.

3.3 Elastic portion of deformation - strain amplitudes

The elastic portions of deformation measured in the long-term cyclic tests are inspected in Figure 10. The curves of axial strain amplitude $\varepsilon_1^{\mathrm{ampl}}(N)$ for the uniform materials L2 to L7 are presented in Figure 10a, while those for the sands L4 and L10 to L16 with varying uniformity coefficients are grouped in Figure 10b. In accordance with earlier test series [27, 31], for most materials a decrease of the strain amplitude during the first 100 cycles was observed, in particular in the tests with the larger stress amplitudes $q^{\mathrm{ampl}} = 60$ and 80 kPa (e.g. in the test on L4, Figure 10a,b). This initial decrease was followed by a phase ($100 \leq N \leq 10^5$) with nearly constant or even slightly in-

1	2	3	4	5	6	7	8	9	10	11	12	13	14
Sand	Parameters from tests with 10^5 cycles, adapted from [31]							Parameters from tests with $2 \cdot 10^6$ cycles with C_{ampl}, C_e, C_p, C_Y from					
								columns 2-5			Eqs. (4) to (7)		
	C_{ampl} [-]	C_e [-]	C_p [-]	C_Y [-]	C_{N1} [10^{-4}]	C_{N2} [-]	C_{N3} [10^{-5}]	C_{N1} [10^{-4}]	C_{N2} [-]	C_{N3} [10^{-5}]	C_{N1} [10^{-4}]	C_{N2} [-]	C_{N3} [10^{-5}]
L2	1.33	0.65	0.30	1.89	18.0	0.15	6.0	32.8	0,012	0.75	10.4	0.017	0.65
L3	1.85	0.61	0.55	3.00	8.25	0.24	2.1	7.36	0,160	0.80	5.90	0.175	0.70
L4	1.97	0.57	0.52	2.82	4.35	0.30	3.5	4.44	0,185	0.95	4.42	0.200	0.90
L5	1.84	0.54	0.32	3.14	2.50	0.54	2.0	2.32	0,260	0.60	3.44	0.260	0.60
L6	1.64	0.58	0.11	2.72	3.66	0.89	0.1	3.50	0,400	0.30	2.70	0.420	0.30
L7	1.48	0.51	0.09	3.49	1.28	0.96	0	1.00	0,720	0.18	1.60	0.720	0.22
L10	1.67	0.53	0.32	2.37	13.4	0.075	5.5	17.0	0.0360	1.80	15.4	0.0240	1.40
L11	2.43	0.53	0.50	2.89	15.4	0.040	13.5	16.0	0.0400	5.00	17.6	0.0450	2.50
L12	1.60	0.48	0.44	3.02	36.0	0.016	10.5	52.0	0.0080	3.00	43.2	0.0070	2.00
L13	1.85	0.40	0.34	3.12	26.6	0.0090	10.0	46.8	0.0060	2.00	46.8	0.0160	2.50
L14	2.34	0.34	0.45	3.29	23.0	0.0065	7.5	42.2	0.0065	1.60	89.4	0.0050	2.50
L15	1.97	0.34	0.44	2.69	41.2	0.0070	7.5	120.0	0.0020	1.20	130.0	0.0045	3.50
L16	1.53	0.31	0.23	2.45	79.2	0.0050	8.0	160.0	0.0020	1.20	142.0	0.0070	5.00

Table 2: HCA model parameters for the 13 tested sands.

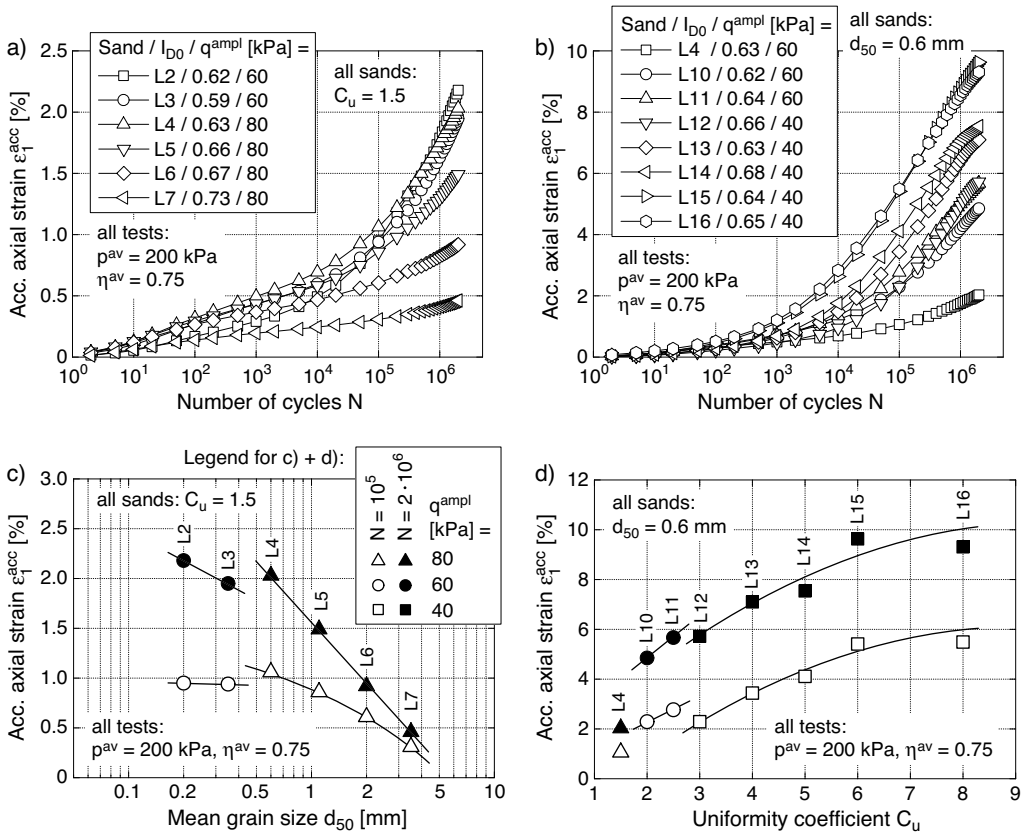

Fig. 8: *Curves $\varepsilon_1^{acc}(N)$ in tests on sands with a) C_u = 1.5 and varying d_{50} (L2 - L7) and b) d_{50} = 0.6 mm and varying C_u (L4, L10 - L16); Accumulated axial strain ε_1^{acc} after 100,000 (empty symbols) and 2 million cycles (filled symbols) as a function of c) mean grain size d_{50} and d) uniformity coefficient C_u*

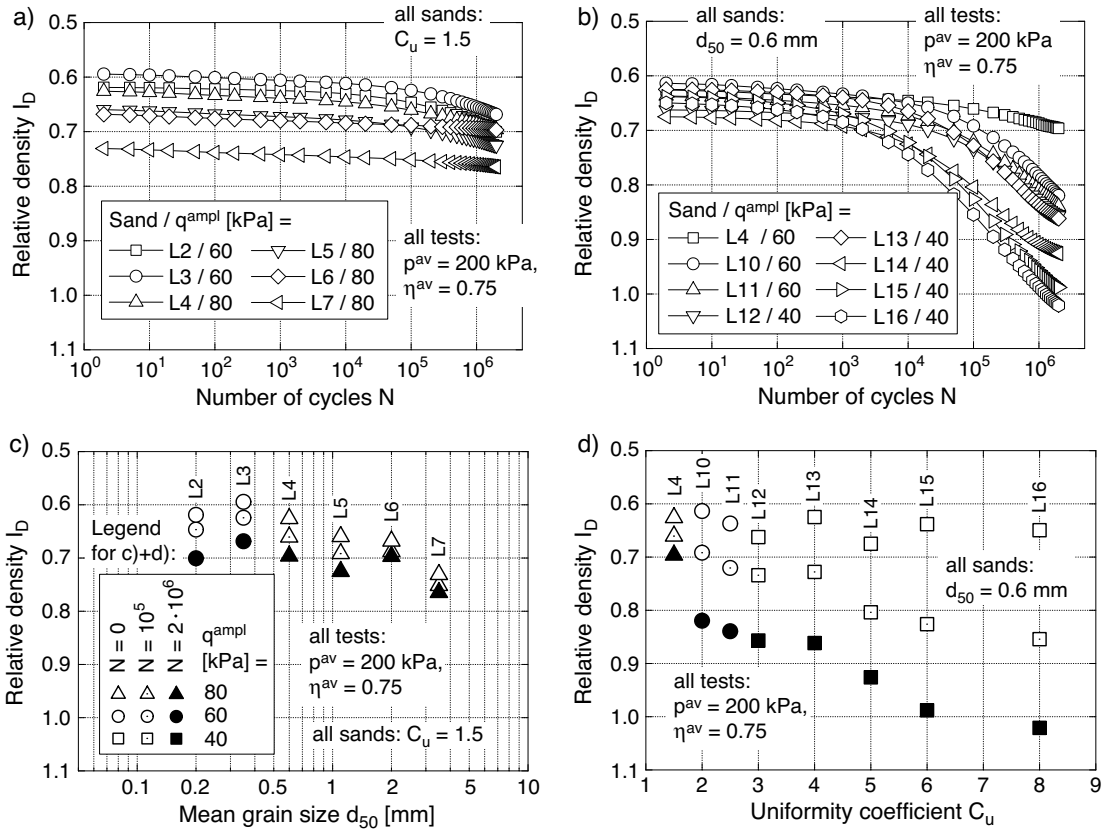

Fig. 9: *Development of relative density I_D with increasing number of cycles in tests on sands with a) C_u = 1.5 and varying d_{50} (L2 - L7) and b) d_{50} = 0.6 mm and varying C_u (L4, L10 - L16); Relative density I_D at N = 0, 10^5 and $2 \cdot 10^6$ as a function of c) mean grain size d_{50} and d) uniformity coefficient C_u*

creasing strain amplitudes ε_1^{ampl}. A moderate re-increase was particularly measured for the more well graded granular materials loaded with the smallest tested stress amplitude q^{ampl} = 40 kPa (e.g. for L16, Figure 10b). Finally, for all tested materials ε_1^{ampl} significantly decreased with N between $N = 10^5$ and $N = 2 \cdot 10^6$. While this final reduction of ε_1^{ampl} may be due to compaction of the sand, the initial decrease ($N < 100$) and the intermediate re-increase observed for some materials cannot be explained by void ratio changes. These ε_1^{ampl} variations are most likely caused by an alteration of the sand fabric or by changes in the force transmission chains within the skeleton of grains. The micromechanical mechanisms leading to these experimental observations are not fully understood yet and need further research.

The influence of the grain size distribution curve on the elastic strains is examined in Figure 10c,d. The axial strain amplitude at $N = 10^5$ (empty symbols) and $N = 2 \cdot 10^6$ (filled symbols) is plotted versus d_{50} or C_u, respectively. The decrease of the strain amplitude between $N = 10^5$ and $N = 2 \cdot 10^6$ is obvious in these diagrams, since all filled symbols lie considerably below the corresponding empty ones. Looking at the uniform sands L4 to L7 loaded with q^{ampl} = 80 kPa, the largest strain amplitude and thus the lowest secant stiffness has been observed at d_{50} = 1 mm (Figure 10c). The decrease of ε_1^{ampl} with increasing mean grain size at $d_{50} > 1$ mm may be partly attributed to the higher initial densities in the tests on the coarser materials. For a constant stress amplitude, the strain amplitudes at $N = 10^5$ do hardly depend on the uniformity coefficient (Figure 10d), while a slight decrease of ε_1^{ampl} with increasing C_u can be concluded from the data for $N = 2 \cdot 10^6$.

It should be noted that tests with similar initial densities have been analyzed in Figure 10. If the tests would have been performed with a constant void ratio instead of density, a significant reduction of the secant stiffness with increasing uniformity coefficient could be expected [33,34].

4 Simplified HCA model calibration with correlations extended for 2 million cycles

In [31], for a simplified calibration of the HCA model parameters in the absence of cyclic test data, the following correlations of the parameters with index properties (d_{50}, C_u, e_{min}) have been proposed:

$$C_{ampl} = 1.70 \quad (4)$$

$$C_e = 0.95 \cdot e_{min} \quad (5)$$

$$C_p = 0.41 \cdot [1 - 0.34\ (d_{50} - 0.6)] \quad (6)$$

$$C_Y = 2.60 \cdot [1 + 0.12\ \ln(d_{50}/0.6)] \quad (7)$$

$$\begin{aligned} C_{N1} &= 4.5 \cdot 10^{-4} \cdot [1 - 0.306\ \ln(d_{50}/0.6)] \\ &\quad \cdot [1 + 3.15\ (C_u - 1.5)] \\ &= 0.00120\ [1 - 0.36 \ln(d_{50})]\ (C_u - 1.18) \end{aligned} \quad (8)$$

$$\begin{aligned} C_{N2} &= 0.31\ \exp[0.39\ (d_{50} - 0.6)] \\ &\quad \cdot \exp\{12.3[\exp(-0.77 C_u) - 0.315]\} \\ &= 0.0051\ \exp[0.39 d_{50} + 12.3 \exp(-0.77 C_u)] \end{aligned} \quad (9)$$

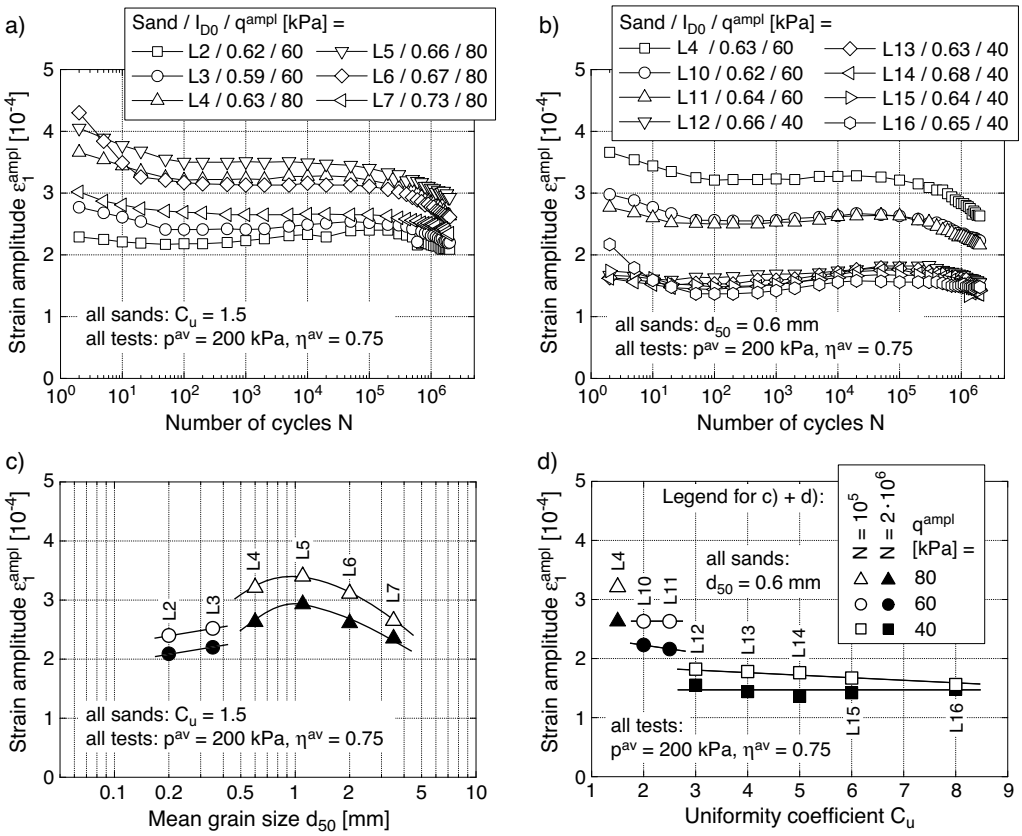

Fig. 10: *Curves $\varepsilon_1^{ampl}(N)$ in tests on sands with a) C_u = 1.5 and varying d_{50} (L2 - L7) and b) d_{50} = 0.6 mm and varying C_u (L4, L10 - L16); Axial strain amplitude ε_1^{ampl} at $N = 10^5$ (empty symbols) and $N = 2 \cdot 10^6$ (filled symbols) as a function of c) mean grain size d_{50} and d) uniformity coefficient C_u*

$$\begin{aligned} C_{N3} &= 3.0 \cdot 10^{-5} \cdot \exp[-0.84\ (d_{50} - 0.6)] \\ &\quad \cdot [1 + 7.85\ (C_u - 1.5)]^{0.34} \\ &= 1.00 \cdot 10^{-4} \cdot \exp(-0.84\ d_{50})(C_u - 1.37)^{0.34} \end{aligned} \tag{10}$$

where d_{50} has to be inserted in [mm]. These correlations were developed based on the data from numerous tests with 10^5 cycles. The data from the new long-term cyclic tests allow the examination of the correlations given by Eqs. (8) to (10) for $2 \cdot 10^6$ cycles.

With the parameters C_{ampl}, C_e, C_p and C_Y calculated from the correlations (4) to (7), another curve-fitting has been performed to the long-term test data delivering the parameters C_{N1}, C_{N2} and C_{N3} given in columns 12 to 14 of Table 2. The accumulation curves $\varepsilon_1^{\text{acc}}$ predicted by the HCA model using these parameters are practically identical with the solid curves provided in Figure 7.

In Figure 11 these parameters are plotted versus the mean grain size d_{50} (data of L2 to L7) or the uniformity coefficient C_u (data of L4 and L10 to L16), respectively. Eqs. (8) to (10) have been added as dashed curves in Figure 11. Obviously, the C_{N3}-values obtained from the long-term cyclic tests are significantly smaller than those calculated from Eq. (10) (Figure 11e,f). Furthermore, the parameters C_{N2} derived for 2 million cycles are also lying slightly below those predicted by Eq. (9) (Figure 11c,d).

In comparison to the other tested materials, for sand L2 (d_{50} = 0.2 mm, C_u = 1.5) an unexpectedly small C_{N2} value (Figure 11c) and consequently a relatively large C_{N1} value was obtained (Figure 11a). In the earlier study with 100,000 cycles documented in [31] the experimental data for sand L2 did not show any distinct deviations from the data measured for the other poorly graded sands. Furthermore, with the exception of L2, although differing in magnitude, the trends of the parameters C_{N1}, C_{N2} and C_{N3} with d_{50} and C_u in Figure 11 are similar to those derived from the tests with 10^5 cycles [31]. The reasons for the deviations in case of sand L2 are not clear yet. Therefore, the C_{N1} and C_{N2} values for L2 are treated as outliers in the following analysis. Neglecting these outliers, the C_{N1}-d_{50}-relationship obtained from the long-term cyclic tests is similar to that reported in [31] (Figure 11a), while the C_{N1}-C_u curve for $N = 2 \cdot 10^6$ is somewhat steeper than for $N = 10^5$ (Figure 11b).

The parameters C_{N1}, C_{N2} and C_{N3} obtained from the long-term tests with 2 million cycles can be approximated by correlations similar to Eqs. (8) to (10) but with different coefficients:

$$C_{N1} = 0.00184\ [1 - 0.47 \ln(d_{50})]\ (C_u - 1.30) \tag{11}$$

$$C_{N2} = 0.00434\ \exp[0.42 d_{50} + 13.0 \exp(-0.85 C_u)] \tag{12}$$

$$C_{N3} = 1.83 \cdot 10^{-5} \cdot \exp(-0.37\ d_{50})(C_u - 1.23)^{0.59} \tag{13}$$

These correlations are given as thick solid curves in Figure 11. Due to the larger deviations the data for sand L2 have been neglected in the development of Eqs. (11) to (13).

For a simplified calibration of the HCA model parameters, Eqs. (8) to (10) are recommended for boundary value problems with $N \leq 10^5$ cycles while Eqs. (11) to (13) are more suitable for larger numbers of cycles ($10^5 < N \leq 2 \cdot 10^6$).

Generally, if the HCA model parameters are calibrated from cyclic test data instead of using the correlation equations (8) to (10) or (11) to (13), the maximum number of cycles in these tests should be chosen representative for the cyclic loading of the practical problem under consideration.

5 Summary, conclusions and outlook

13 drained cyclic triaxial tests with 2 million cycles have been performed on clean quartz sand. Different grain size distribution curves with mean grain sizes in the range 0.2 mm $\leq d_{50} \leq$ 3.5 mm and uniformity coefficients $1.5 \leq C_u \leq 8$ have been tested.

From earlier tests with only 10^5 cycles it was already known that the accumulation curves $\varepsilon_1^{\mathrm{acc}}(N)$ of poorly graded sands usually obey $\varepsilon_1^{\mathrm{acc}} \sim \ln(N)$ up to $N \approx 10^4$. In the range $10^4 < N \leq 10^5$ the inclination of the accumulation curves (plotted in a semi-logarithmic $\varepsilon_1^{\mathrm{acc}}$-$N$ diagram) usually increases. The new long-term tests show that this increase continues even up to $N = 2 \cdot 10^6$ cycles. Furthermore, such increase in the range $10^5 < N \leq 2 \cdot 10^6$ was measured also for coarse sands and fine gravels where the accumulation curves followed $\varepsilon^{\mathrm{acc}} \sim \ln(N)$ during the first 10^5 cycles. For most of the more well-graded sands the accumulation curves $\varepsilon_1^{\mathrm{acc}}(N)$ showed a pronounced bending in the semi-logarithmic diagrams at $N \leq 10^5$ while the curves were almost linear at larger numbers of cycles ($10^5 < N \leq 2{\cdot}10^6$). For some of the well-graded materials a decrease of the rate of accumulation at larger N-values lead to S-shaped accumulation curves in the semi-logarithmic scale.

Despite the different shape, the measured accumulation curves for the various sands can be well approximated by the function $\varepsilon^{\mathrm{acc}} \sim f_N = C_{N1}\left[\ln(1 + C_{N2}N) + C_{N3}N\right]$ of the HCA model proposed by Niemunis et al. [16]. This function was originally developed based on data from tests with 10^5 cycles only. The new test data reveals that f_N is suitable at least up to $N = 2{\cdot}10^6$ cycles. However, the test data at $N > 10^6$ occasionally give hints that this conclusion may not be valid for even larger number of cycles $N > 2 \cdot 10^6$, because the decay of the rate of strain accumulation at large N values was observed faster than predicted by f_N for some more well-graded materials.

Recalculations of the new long term tests with 2 million cycles using the HCA model with parameters calibrated from an earlier test series with $N = 10^5$ cycles performed on the same sands (parameters adapted from [31]) showed a good prediction of the measured cumulative deformations in the range $N \leq 10^5$. At larger numbers of cycles, however, the measured strain accumulation rates are significantly overestimated by these parameters. Therefore, new parameters C_{N1}, C_{N2} and C_{N3} have been calibrated based on the long-term test data.

The correlations between the HCA model parameters C_{N1}, C_{N2} and C_{N3} and the granulometry (d_{50}, C_u) proposed in [31] for 10^5 cycles have been inspected based on the new long-term test data. In particular, the parameters C_{N3} calibrated from the tests with 2 million cycles were found significantly lower than those calculated from the previous correlation equation. Based on the long-term test data, modified correlation equations for C_{N1}, C_{N2} and C_{N3} have been developed. They may be applied for a simplified calibration of the HCA model parameters in the case of boundary value problems with $10^5 < N \leq 2 \cdot 10^6$ cycles.

The data from the long-term tests have also been used to inspect the high-cyclic flow rule **m** used in the HCA model. The ratio of the volumetric and deviatoric strain accumulation rates measured in the range $10^5 < N \leq 2{\cdot}10^6$ was found similar to that observed for smaller numbers of cycles. Therefore, the high-cyclic flow rule **m** validated up to 10^5 cycles so far [30] is applicable also to larger numbers of cycles.

As already mentioned in [31], the correlations (4) to (13) should only be applied within the range of tested d_{50}- and C_u-values, i.e. 0.2 mm $\leq d_{50} \leq$ 3.5 mm and $1.5 \leq C_u \leq 8$ in case of the equations derived from the long-term cyclic tests. Furthermore, at present these correlations are only valid for clean quartz sands with subangular grain shape.

It is intended to extend the correlations (4) to (13) in order to consider the influences of a fines content (up to now only clean quartz sands have been tested) and of the grain characteristics (e.g. shape, surface roughness, mineralogy). The respective experimental study will be presented in a separate publication in future.

Acknowledgement

The experiments analyzed in the paper have been performed during the former work of the authors at Ruhr-University Bochum (RUB), Germany. The tests were conducted by the laboratory technician M. Skubisch. The analysis of the test results has been undertaken at IBF, KIT in the framework of the project "Improvement of an accumulation model for high-cyclic loading" (TR 218/18-1). The authors are grateful to DFG (German Research Council) for the financial support.

References

[1] M. Abdelkrim, P. De Buhan, and G. Bonnet. A general method for calculating the traffic load-induced residual settlement of a platform, based on a structural analysis approach. *Soils and Foundations*, 46(4):401–414, 2006.

[2] M. Achmus, Y.-S. Kuo, and A. Abdel-Rahman. Zur Bemessung von Monopiles für zyklische Lasten. *Der Bauingenieur*, 83:303–311, 2008.

[3] G. Bouckovalas, R.V. Whitman, and W.A. Marr. Permanent displacement of sand with cyclic loading. *Journal of Geotechnical Engineering, ASCE*, 110(11):1606–1623, 1984.

[4] G. Festag. Experimentelle und numerische Untersuchungen zum Verhalten von granularen Materialien unter zyklischer Beanspruchung. Mitteilungen des Instituts und der Versuchsanstalt für Geotechnik, Technische Universität Darmstadt, Heft 66, 2005.

[5] G. Gidel, D. Breysse, P. Hornych, J.-J. Chauvin, and A. Denis. A new approach for investigating the permanent deformation behaviour of unbound granular material using the repeated load triaxial apparatus. *Bulletin des Laboratoires des Ponts et Chaussées*, 233(4):5–21, 2001.

[6] A. Gotschol and H.-G. Kempfert. Zyklisch viskoelastisch-viskoplastischer Stoffansatz nichtbindiger Böden und Schotter. *Bautechnik*, 81(4):279–285, 2004.

[7] J. Helm, J. Laue, and Th. Triantafyllidis. Untersuchungen an der RUB zur Verformungsentwicklung von Böden

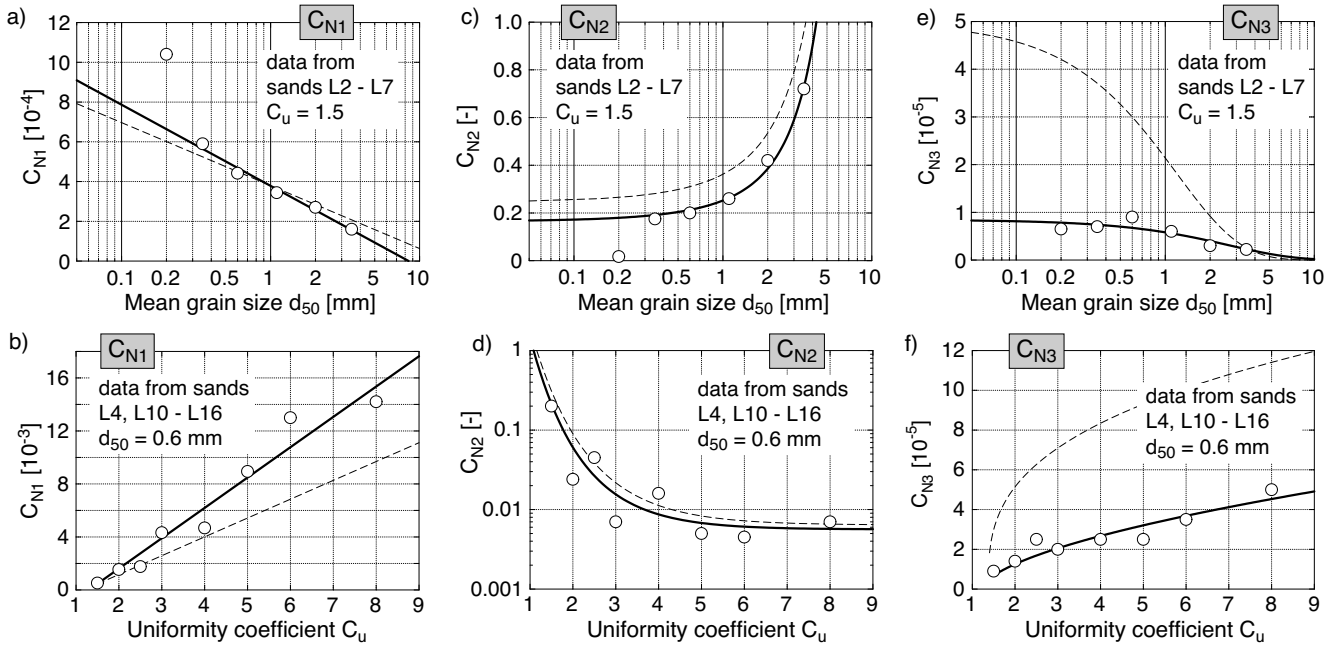

Fig. 11: *Correlations of HCA model parameters C_{N1}, C_{N2} and C_{N3} with mean grain size d_{50} and uniformity coefficient C_u. Dashed curves: Eqs. (8) to (10); Solid curves: Eqs. (11) to (13)*

unter zyklischen Belastungen. In *Beiträge zum Workshop: Boden unter fast zyklischer Belastung: Erfahrungen und Forschungsergebnisse, Veröffentlichungen des Institutes für Grundbau und Bodenmechanik, Ruhr-Universität Bochum, Heft Nr. 32*, pages 201–222, 2000.

[8] A. Hettler. Verschiebungen starrer und elastischer Gründungskörper in Sand bei monotoner und zyklischer Belastung. Institut für Boden- und Felsmechanik der Universität Karlsruhe, Heft Nr. 90, 1981.

[9] U. Holzlöhner. Bleibende Setzung von Fundamenten infolge dynamischer Last. *Bautechnik*, 55:150–154, 1978.

[10] M. Huurman. *Permanent deformation in concrete block pavements*. PhD thesis, Delft University of Technology, 1997.

[11] C. Karg, S. Francois, W. Haegeman, and G. Degrande. Elasto-plastic long-term behavior of granular soils: modeling and experimental validation. *Soil Dynamics and Earthquake Engineering*, 30(8):635–646, 2010.

[12] J. Laue. Zur Setzung von Flachfundamenten auf Sand unter wiederholten Lastereignissen. Dissertation, Veröffentlichungen des Institutes für Grundbau und Bodenmechanik, Ruhr-Universität Bochum, Heft Nr. 25, 1996.

[13] C. Leblanc, G.T. Houlsby, and B.W. Byrne. Response of stiff piles in sand to long-term cyclic lateral loading. *Géotechnique*, 60(2):79–90, 2010.

[14] F. Lekarp, U. Isacsson, and A. Dawson. State of the art. II: Permanent strain response of unbound aggregates. *Journal of Transportation Engineering*, 126(1):76–83, 2000.

[15] W.A. Marr and J.T. Christian. Permanent displacements due to cyclic wave loading. *Journal of the Geotechnical Engineering Division, ASCE*, 107(GT8):1129–1149, 1981.

[16] A. Niemunis, T. Wichtmann, and T. Triantafyllidis. A high-cycle accumulation model for sand. *Computers and Geotechnics*, 32(4):245–263, 2005.

[17] C. Pasten, H. Shin, and J.C. Santamarina. Long-Term Foundation Response to Repetitive Loading. *Journal of Geotechnical and Geoenvironmental Engineering, ASCE*, 140(4), 2014.

[18] A.J. Puppala, S. Saride, and S. Chomtid. Experimental and Modeling Studies of Permanent Strains of Subgrade Soils. *Journal of Transportation Engineering*, 135(10):1379–1389, 2009.

[19] G.P. Raymond and F. El Komos. Repeated load testing of a model plane strain footing. *Canadian Geotechnical Journal*, 15:190–201, 1978.

[20] A. Sawicki and W. Świdziński. Compaction curve as one of basic characteristics of granular soils. In E. Flavigny and D. Cordary, editors, *4th Colloque Franco-Polonais de Mechanique des Sols Appliquee*, volume 1, pages 103–115, 1987. Grenoble.

[21] A. Sawicki and W. Świdziński. Mechanics of a sandy subsoil subjected to cyclic loadings. *Int. J. Numer. Anal. Meth. Geomech.*, 13:511–529, 1989.

[22] A.S.J. Suiker and R. de Borst. A numerical model for the cyclic deterioration of railway tracks. *International Journal for Numerical Methods in Engineering*, 57:441–470, 2003.

[23] A.S.J. Suiker, E.T. Selig, and R. Frenkel. Static and cyclic triaxial testing of ballast and subballast. *Journal of Geotechnical and Geoenvironmental Engineering, ASCE*, 131(6):771–782, 2005.

[24] H.E. Taşan, F. Rackwitz, and R. Glasenapp. Ein Bemessungsmodell für Monopilegründungen unter zyklischen Horizontallasten. *Bautechnik*, 88(5):301–318, 2011.

[25] J. Uzan. Permanent Deformation in Flexible Pavements. *Journal of Transportation Engineering*, 130(1):6 – 13, 2004.

[26] S. Werkmeister. *Permanent Deformation Behaviour of Unbound Granular Materials in Pavement Constructions*. PhD thesis, Technical University Dresden, 2003.

[27] T. Wichtmann, A. Niemunis, and T. Triantafyllidis. Strain accumulation in sand due to cyclic loading: drained triaxial tests. *Soil Dynamics and Earthquake Engineering*, 25(12):967–979, 2005.

[28] T. Wichtmann, A. Niemunis, and T. Triantafyllidis. Validation and calibration of a high-cycle accumulation model based on cyclic triaxial tests on eight sands. *Soils and Foundations*, 49(5):711–728, 2009.

[29] T. Wichtmann, A. Niemunis, and T. Triantafyllidis. On the determination of a set of material constants for a high-cycle accumulation model for non-cohesive soils. *Int. J. Numer. Anal. Meth. Geomech.*, 34(4):409–440, 2010.

[30] T. Wichtmann, A. Niemunis, and T. Triantafyllidis. Flow rule in a high-cycle accumulation model backed by cyclic test data of 22 sands. *Acta Geotechnica*, 9(4):695–709, 2014.

[31] T. Wichtmann, A. Niemunis, and T. Triantafyllidis. Improved simplified calibration procedure for a high-cycle accumulation model. *Soil Dynamics and Earthquake Engineering*, 70(3):118–132, 2015.

[32] T. Wichtmann, H.A. Rondón, A. Niemunis, T. Triantafyllidis, and A. Lizcano. Prediction of permanent deformations in pavements using a high-cycle accumulation model. *Journal of Geotechnical and Geoenvironmental Engineering, ASCE*, 136(5):728–740, 2010.

[33] T. Wichtmann and T. Triantafyllidis. Influence of the grain size distribution curve of quartz sand on the small strain shear modulus $G_{\max}$. *Journal of Geotechnical and Geoenvironmental Engineering, ASCE*, 135(10):1404–1418, 2009.

[34] T. Wichtmann and T. Triantafyllidis. Effect of uniformity coefficient on $G/G_{\max}$ and damping ratio of uniform to well graded quartz sands. *Journal of Geotechnical and Geoenvironmental Engineering, ASCE*, 139(1):59–72, 2013.